LANGMUIR

Article

pubs.acs.org/Langmuir

Interfacial Rheology of Sterically Stabilized Colloids at Liquid Interfaces and Its Effect on the Stability of Pickering Emulsions

Rob Van Hooghten,[†,∥] Victoria E. Blair,[‡] Anja Vananroye,[†] Andrew B. Schofield,[§] Jan Vermant,[‡] and Job H. J. Thijssen*[,§]

[†]Department of Chemical Engineering, KU Leuven, Celestijnenlaan 200F, Leuven B-3001, Belgium

[‡]Department of Materials, ETH Zürich, Vladimir-Prelog-Weg 5, Zürich CH-8093, Switzerland

[§]SUPA School of Physics & Astronomy, The University of Edinburgh, Edinburgh EH9 3FD, United Kingdom

Supporting Information

ABSTRACT: Particle-laden interfaces can be used to stabilize a variety of high-interface systems, from foams over emulsions to polymer blends. The relation between the particle interactions, the structure and rheology of the interface, and the stability of the system remains unclear. In the present work, we experimentally investigate how micron-sized, near-hard-sphere-like particles affect the mechanical properties of liquid interfaces. In particular, by comparing dried and undried samples, we investigate the effect of aggregation state on the properties of the particle-laden liquid interface and its relation to the stability of the corresponding Pickering emulsions. Partially aggregated suspensions give rise to a soft-solid-like response under shear, whereas for stable PMMA particulate layers a liquid-like behavior is observed. For interfacial creep-recovery measurements, we present an empirical method to correct for the combined effect of the subphase drag and the compliance of the double-wall ring geometry, which makes a significant contribution to the apparent elasticity of weak interfaces. We further demonstrate that both undried and dried PMMA particles can stabilize emulsions for months, dispelling the notion that particle aggregation, in bulk or at the interface, is required to create stable Pickering emulsions. Our results indicate that shear rheology is a sensitive probe of colloidal interactions but is not necessarily a predictor of the stability of interfaces, e.g., in quiescent Pickering emulsions, as in the latter the response to dilatational deformations can be of prime importance.

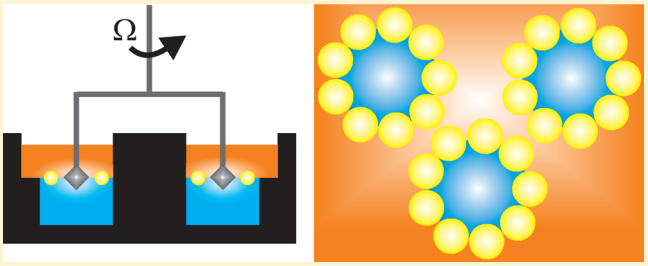

INTRODUCTION

In fluid−fluid composites, the mechanical properties of the interface between the two phases are of crucial importance to the shelf life and flow properties of the material as a whole.[1−3] A striking example of this is particle-stabilized emulsions, i.e., dispersions of droplets in an immiscible liquid stabilized by colloidal particles rather than molecular surfactants,[4] as they can display solid-like behavior even though they are comprised almost entirely of liquids.[2,5] In recent years, these so-called Pickering−Ramsden (PR) emulsions have received growing attention, because they are (i) model arrested systems, (ii) ubiquitous in a range of industries spanning foods to petrochemicals, and (iii) promising as templates for advanced porous materials.[6−9] Despite these efforts, open questions remain regarding the stability of PR emulsions in both quiescent and out-of-equilibrium conditions.[10−14]

An important difference between molecular surfactants and colloidal particles at liquid interfaces is that the former reduce the interfacial energy by reducing the interfacial tension γ whereas the latter do so by reducing the liquid−liquid contact area A. This is quantified by the detachment energy

$$\Delta G_d = \pi R^2 \gamma (1 - |\cos\theta|)^2 \quad (1)$$

where R is the radius of the particle and θ is its three-phase contact angle.[15] For a 0.5 μm radius (PMMA) sphere at a water−alkane interface, i.e., $\gamma \approx 50$ mN m^{-1} and $\theta \approx 150°$,[16−18] this detachment energy $\Delta G_d \approx 7.0 \times 10^{-16}$ J $\approx 1.7 \times 10^5\ k_B T_{room}$ (Boltzmann constant[19] k_B and room temperature T_{room}). This means that, unlike molecular surfactants, these colloidal particles are irreversibly attached to the liquid interface.[20] In emulsions, provided the surface coverage is sufficient, such interfacial particles provide a mechanical barrier to coarsening, which could occur via coalescence and/or Ostwald ripening.[4]

Previous investigations have suggested that the role of particles in stabilizing emulsions and foams can be quantified using the rheology of the particle-laden liquid interface. For example, maxima in compression elastic moduli have been linked to optimum stability of particle-stabilized liquid−air interfaces,[21,22] i.e., highly (visco-)elastic interfaces slow down and/or suppress coarsening. Furthermore, maxima in yield and/or melting strains have been associated with enhanced stability of PR emulsions/foams.[21,22] In this case, coalescence is

Received: December 5, 2016
Revised: February 7, 2017
Published: April 17, 2017

DOI: 10.1021/acs.langmuir.6b04365
Langmuir 2017, 33, 4107−4118

arrested when the strength of the interfacial-particle assembly is enough to withstand droplet collisions (even under shear). However, the full impact of the rheology of the particle-laden interface on the stability of PR composites remains far from fully understood.

The quantitative study of the mechanical properties of (particle-laden) liquid-fluid interfaces is called "interfacial rheology". To study this, various experimental techniques have been reported and, in the interest of conciseness, we refer the reader to appropriate reviews in the literature for an overview.[3,23−25] These methods are often categorized as dilatational (e.g., Langmuir trough[26,27]) or shear (e.g., double-wall ring[28]), depending on whether the liquid-interfacial area is changed or constant during the measurement, even though many proposed devices use mixed deformation modes. Note that it has been observed that the orientation of the Wilhelmy plate can affect the results of Langmuir-trough measurements,[29,30] but it does not affect results for micron-sized particles.[31] In addition to these macroscopic probes, interfacial microrheology aims to extract the mechanical properties of the liquid interface by monitoring the movement of interfacial particles (passive), optionally in response to an external stimulus (active).[32] It should be noted here that results from interfacial micro- and macrorheology on the same system do not always agree and rationalizing the difference is not trivial.[32]

An important quantity to consider in any interfacial-rheology experiment is the Boussinesq number

$$Bo = \frac{\eta_S}{\eta a} \tag{2}$$

in which η is the viscosity of the subphase (water), η_S the viscosity of the interface and a is a geometrical parameter characterizing the measurement geometry.[33] As the Boussinesq number is essentially the ratio of surface and subphase drag, a measurement geometry can only probe the interfacial rheology if $Bo \gg 1$, otherwise the bulk rheology of the subphase will dominate. As an illustrative example, consider a typical double-wall ring setup,[28] for which $a \approx 1$ mm. For typical values of the surface viscosity $\eta_S \approx 10^{-4}$ Pa m s,[22,34]

$$Bo \sim \frac{10^{-4}\text{Pa m s}}{10^{-3}\text{Pa s } 10^{-3}\text{m}} = 10^2 \gg 1 \tag{3}$$

demonstrating the feasibility of such measurements.

In addition to interfacial tension and particle-liquid interactions, interfacial rheology also depends on interparticle interactions. For example, Christopher and co-workers linked how the microstructure of aggregated densely packed interfaces creates a percolated solid-like regime for surface concentrations well below maximum packing fraction, which creates a yield-stress interface (with the nature of the shear thinning depending on surface concentration).[35] They subsequently showed how the dynamic arrest in the microstructure in aggregated suspensions of polystyrene colloids is affected both by capillary attraction between particles and local effects due to increased surface coverage.[36] To the best of our knowledge, these and other previous investigations have mostly considered charge-stabilized particles. This has made the interpretation of experimental results difficult, as the charge distribution around interfacial colloids is nonisotropic.[37,38] In an attempt to simplify the system under consideration, we focus instead on sterically stabilized particles, i.e., particles that behave like near-hard spheres in the (continuous) oil phase.[39,40]

Here we present a comprehensive set of interfacial experiments, using both microscopy and rheology, on poly(methyl methacrylate) (PMMA) particles at water−oil interfaces. We find that, under shear, interfacial aggregates of dried particles endow the liquid interface with the mechanical properties of a weak 2D solid, whereas nonaggregated (undried) particles result in a response close to that of the liquid interface itself.[41] To properly analyze interfacial creep-recovery data of such weakly elastic interfaces, we present an empirical method to correct for the combined effect of the subphase drag and the compliance of the measurement geometry. In compression−expansion experiments, we find that liquid interfaces laden with undried or dried particles behave similarly upon initial compression and develop clearly nonzero surface pressures when approaching close-packing. Finally, we demonstrate that both undried and dried particles can stabilize emulsions for months, and that the particles on the droplets do not form brittle layers, thereby dispelling the notion that aggregating particles are a necessary condition to create stable PR emulsions.[10,11,42−44] We suggest that systems in which shear-interfacial rheology dominates, aggregating particles can create solid-like interfaces that enhance the stability of PR emulsions;[34] in systems such as we investigate here, wherein dilatational rheology dominates, PR emulsions can be stable without aggregating particles.

EXPERIMENTAL SECTION

Materials. In Edinburgh, distilled water was passed through a Millipore Milli-Q RG system before use (resistivity 18 MΩ cm). *n*-Hexadecane (Sigma-Aldrich, ReagentPlus, 99%) was filtered twice through alumina powder (Sigma-Aldrich, activated) to remove polar impurities. The purity of these two liquid phases was checked by measuring their surface tension vs air in a pendant-drop tensiometer (Krüss EasyDrop, model FM40Mk2): 72.5 mN m^{-1} for the water and 27.5 mN m^{-1} for the oil, which compares favorably with literature values.[45,46] For the optical micrographs comparing undried and dried particles, *n*-dodecane (Acros Organics, 99%) was filtered three times through alumina powder. For the index-matched PR emulsions (see below), these additional materials were used: sodium iodide (Sigma-Aldrich, ≥99.5%), poly(dimethylsiloxane-*co*-methylphenylsiloxane (DC550, Aldrich, Dow Corning 550 fluid), and cycloheptyl bromide (CHB, Aldrich, 97%).

A similar procedure was followed in Leuven and Zürich. *n*-Hexadecane (Acros Organics, 99%, pure) was filtered twice through alumina powder (Sigma-Aldrich, activated). In Zürich, ultrapure water was acquired from a Milli-Q Advantage A10 system (resistivity 18 MΩ cm). In Leuven, distilled water was passed through a Sartorius Arium 611 DI system (resistivity 18 MΩ cm). Interfacial tensions of both liquid phases were checked with a pendant-drop tensiometer (KSV Instruments, CAM200).

As in refs 5 and 17, poly(methyl methacrylate) (PMMA) particles, stabilized by a layer of poly(12-hydroxystearic acid) (PHSA), were synthesized following Bosma et al.[39] They were labeled with the fluorescent dye 4-chloro-7-nitrobenzo-2-oxa-1,3-diazol (NBD), which was chemically linked to the PMMA during particle synthesis. Three different particle batches were used: (ASM360) radius $R = 0.575$ μm and polydispersity PD = 5%, (ASM408) $R = 1.1$ μm and PD = 2%, and (ASM306) $R = 0.455$ μm and PD = 8% (static light scattering). Undried particles were cleaned by repeated centrifugation/redispersion, first in *n*-dodecane (5×) and then in *n*-hexane (5×) for spreading or *n*-hexadecane (5×) for emulsions. Dried particles were washed in *n*-hexane (10×), followed by drying under vacuum in a Gallenkamp vacuum oven at (43 ± 3) °C. For the Langmuir-trough measurements, particles were first air-dried from *n*-hexane and then vacuum-dried at 40 °C for 2 h. To further investigate the effect of drying, some particles were dried more intensely with a longer vacuum treatment in a vacuum oven (Sheldon, Shel Lab 1410).

DOI: 10.1021/acs.langmuir.6b04365
Langmuir 2017, 33, 4107−4118

It is worth noting here that the contact angle θ of PMMA–PHSA vs water-alkane has been investigated previously. For undried PMMA–PHSA particles on a water-decane interface, Isa et al. measured θ = 129.8° ± 11.8° using freeze-fracture shadow-casting cryo-scanning electron microscopy and θ = 157.4° ± 6.6° using a gel-trapping technique.[18,47,48] Thijssen et al. obtained a value of θ = 160.3° ± 0.4° for a water droplet on a PMMA–PHSA surface under *n*-dodecane;[17] the PMMA–PHSA layers were obtained by spin-coating, during which the solvent evaporates so these are not undried, but they were not treated in a vacuum oven. Judging from their methods section, Wang et al. have kept their PMMA–PHSA particles suspended at all times, i.e., their θ = 150° at water-decane is for undried particles. Comparing these values for θ, we have no reason to suspect that drying the particles has a substantial effect on their contact angle.

Interfacial Microscopy. Glassware was cleaned by soaking in 1 M NaOH(aq) overnight, followed by rinsing with distilled water and drying in an oven at ∼50 °C. In addition, the glass basin for holding the water–oil interface was treated with silanization solution I (Sigma-Aldrich, ∼5% dimethyldichlorosilane in heptane) for 3 h, followed by rinsing with hexane and drying in an oven at ∼50 °C. A total of 10 mL of water was pipetted into the basin, after which 5 mL of *n*-hexadecane was gently deposited onto the water phase.

PMMA–PHSA particles in *n*-hexane were then carefully pipetted onto the oil-air surface; for example 60 μL of 1.27 wt % ASM306 in *n*-hexane was used for Figure 1. This spreading suspension was stored in a fridge at ∼10 °C and redispersed prior to use by 30 s of vortex mixing followed by 30 min in an 80 W ultrasonic bath (VWR) filled with iced water. As the PMMA–PHSA particles did not attach to the hexadecane–air interface, the particles were deposited onto the water–hexadecane interface (checked with microscopy). After spreading, the sample was left on the microscope stage for at least 1 h prior to imaging.

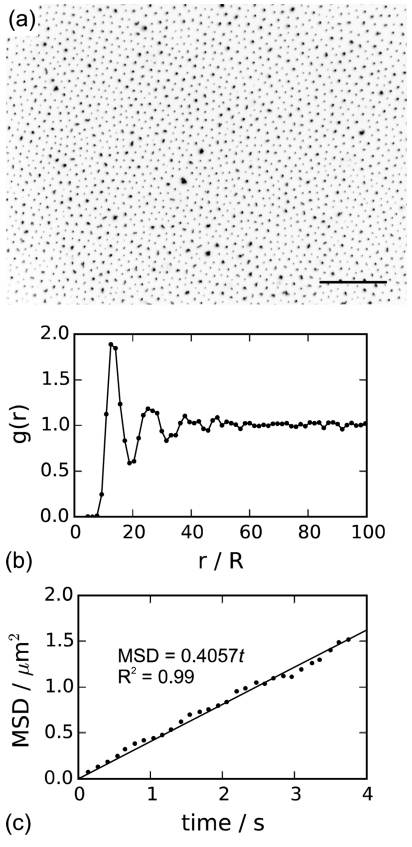

Figure 1. (a) Fluorescence micrograph of undried 0.455 μm radius poly(methyl methacrylate) particles (dark) at a water–oil (hexadecane) interface. Surface coverage expected for perfect deposition is 0.36, measured surface coverage is 0.031, scale bar is 50 μm. (b) Radial distribution function $g(r)$ corresponding to the micrograph in panel (a). (c) Mean squared displacement (averaged over 225 particles) vs time extracted from the corresponding time series after correcting for apparent in-plane drift.

The particle-laden interface was then characterized using a Nikon E800 upright microscope, equipped with a Nikon mercury lamp and a Nikon PF 40 × / 0.60 NA objective. Micrographs were recorded using a Retiga 2000R Fast 1394 camera from QImaging and Proscan software. The microscope, sample and camera were enclosed in a transparent, plastic hood to minimize the effects of air flows. Typically, time sequences were recorded at 7.5 frames per second over 4 s.

Microscopy images were analyzed using the program "Fiji" (ImageJ).[49] For static characterization, images were converted to 8-bit, thresholded (auto) and particle-centroid coordinates were extracted using Fiji's "Analyze particles" feature. These coordinates were then fed to an in-house Python 2.7 code for calculating radial distribution functions; normalization was performed using randomly generated coordinates for the same number of particles. For dynamic characterization, time sequences were first corrected for drift using the "translation" mode of the "StackReg" feature in Fiji. To cope with the large difference in recorded fluorescence intensity between single particles and aggregates, images were thresholded using the "midgrey" mode of the "Auto Local Threshold" feature in Fiji. Particles were then tracked using the Fiji "MTrack2" feature, the output of which was converted to mean-squared displacement in Microsoft Office Excel 2013.

For the comparison of undried vs dried particles, NBD-labeled PMMA–PHSA particles of radius 1.04 μm (DLS) were spread at a water-dodecane interface and the sample was left on the microscope stage for 3 h prior to imaging. Dried particles were dried from dodecane in an oven at 60 °C for 3 h, after which they were dried under vacuum for 2 h until repeated measurements of their mass gave the same result. Fluorescence micrographs were obtained using a Nikon E Plan 20×/0.45 NA ELWD air objective. The NBD in the PMMA particles was excited using a Cool LED pE system and videos were recorded using an Allied Manta camera (MG 033B ASG); emission filters were used as appropriate for NBD fluorescence.

The resulting micrographs were analyzed using the program "Fiji" (ImageJ).[49] To obtain the apparent surface coverage, images were thresholded (auto), after which the area fraction was obtained using the "measure" feature. Subsequently, the "watershed" feature was applied to each image (we visually checked that this does not separate particles in aggregates) and the apparent area of each "entity" (particle or aggregate) was extracted using "Analyze particles". Finally, the average $\langle A \rangle$ and polydispersity $\mathcal{D}$ (eq 4) were calculated in Microsoft Office Excel 2013.

Langmuir Trough. Interfacial compression–expansion experiments were performed at room temperature using a KSV NIMA Langmuir trough (361 × 54 mm^2 total interfacial area and initial barrier separation 300 mm). The PTFE trough and barriers were extensively cleaned with at least three cycles of ethanol, paper tissue, and deionized water prior to use. The surface tension was measured with a Wilhelmy balance (KSV Instruments Ltd.) using a 40 mm circumference Pt plate. Prior to use, the plate was rinsed with acetone or ethanol and flamed using a Bunsen burner. Using this setup, a surface tension of 71.2 to 72.7 mN m^{-1} was measured for a clean water–air interface at room temperature, which agrees favorably with literature values.[45]

Water was then pipetted into the PTFE trough up to a sharp edge 5 mm above the bottom of the trough, which allowed pinning of the water–air interface. Subsequently, an ∼0.5 cm thick layer of *n*-hexadecane (130 mL) was carefully poured onto the water phase. Experiments were only continued if moving the barriers did not substantially change the measured surface tension of the water–oil interface. Dried PMMA–PHSA particles were dispersed into hexane via (2 × 20) min of sonication. Though the resulting suspensions were clear to the eye, i.e., no large aggregates were present, some small aggregates were observed in microscopy (Olympus BX51WI microscope, mercury lamp and Hamamatsu C8800 CCD camera).

DOI: 10.1021/acs.langmuir.6b04365
Langmuir 2017, 33, 4107–4118

A suspension of 0.455 μm radius PMMA–PHSA particles (ASM306, dried or undried) was then carefully pipetted onto the oil–air surface; 26.5 μL of 1.6 wt % PMMA in hexane was used per cm^2 of water–oil interface. Subsequently, the hexane was allowed to evaporate for at least 1.5 h (longer waiting times did not affect the results). In a typical experiment, barriers were moved over 90 to 125 mm and back at a speed of 5 mm ·min^{-1}, this cycle being repeated 3×. Further compression was not possible in our setup as further reduction of barrier separation was observed to disrupt readings of the Wilhelmy plate on clean water interfaces, presumably due to capillarity effects. Surface pressure Π was calculated from the measurements using $\Pi = \gamma_0 - \gamma$, where $\gamma(\gamma_0)$ is the measured interfacial tension (for the bare water–oil interface).

Oscillatory-Shear Rheology. The shear-rheological properties of the particle-laden interfaces were characterized using a setup similar to the one described in ref 28.[28] The PTFE cup (in-house) was extensively cleaned with deionized water, paper tissue, and again deionized water prior to use; the double-wall ring (DWR) was extensively cleaned with deionized water, ethanol, and again deionized water. The particle-laden interface was prepared by carefully pipetting a suspension of 0.575 μm radius PMMA–PHSA particles (ASM360, dried) onto the oil–air surface; 26.5 μL of 1.6 wt % PMMA in hexane was used per cm^2 of water–oil interface. Note that waiting longer than 1 h between particle spreading and shear-rheological measurement did not significantly change the results.

Consecutive oscillatory frequency-sweep (at 0.1% strain amplitude) and strain-sweep (at 1 rad/s) measurements were performed on a stress-controlled AR-G2 rheometer (TA Instruments) using a DWR fixture. The DWR geometries were manufactured via laser sintering of a platinum–iridium alloy (Layerwise, Belgium). To reach maximum sensitivity, the instrument was carefully calibrated prior to use. Note that subsequently adding additional particles, and repeating the measurement, did not qualitatively change the shear-rheology results.

It should be noted here that our water–hexadecane interfaces laden with PMMA–PHSA particles have a response relatively close to that of the water–oil interface itself. Essentially, useful measurements are a delicate balance between sufficient signal-to-noise and limited contribution of the geometry inertia. As a guide to the reader, we provide a color coding for the oscillatory-shear measurements in Figure 4. We label frequency/strain-ranges as green ("acceptable") if (1) the measured oscillatory stress is at least 10× larger than the oscillatory stress associated with the measurement geometry, (2) the measured oscillatory torque is at least 10× larger than the minimum torque limit of the rheometer, and (3) the raw phase angle is smaller than <90°. Similarly, we label frequency/strain-ranges as orange ("probably acceptable") if: (1 and 2) the ratio is at least 5 and (3) the raw phase angle is smaller than <90°. Finally, we suggest that all other frequency/strain-ranges (labeled as gray) are handled with care.

Creep-Recovery Rheology. The same setup and preparation protocol as described for the oscillatory-shear rheology measurements was used for the creep-recovery experiments. Both undried and dried PMMA particles (ASM306) were measured. The experiments were performed on a stress-controlled DHR-3 rheometer (TA Instruments) equipped with the DWR fixture. Two DWR geometries were used: a standard DWR geometry (I = 2.8 μN m s^2, friction = 0.44 μN m rad^{-1} s^{-1}) as described in ref 28, and a modified "thick" DWR geometry with reinforced vertical struts (I = 4.6 μN m s^2, friction =0.46 μN m rad^{-1} s^{-1}); the latter was expected to have a reduced compliance. Both geometries were manufactured via laser sintering of a platinum–iridium alloy (Layerwise, Belgium). The applied stress during creep was varied between 0.001 and 0.025 mPa m. A time interval of 600 s was used during both the creep and recovery step; it was verified that this was sufficient to reach steady state.

Emulsion Characterization. Sample mixtures for emulsification were prepared with PMMA–PHSA particles (ASM306). In the case of dried particles ("d"), *n*-hexadecane was added to dry powders in clean glass vials. In the case of undried particles ("w"), *n*-hexadecane was used to dilute stock suspensions of PMMA particles in *n*-hexadecane. All these samples were sonicated at 80 W for (3 × 15) minutes, followed by 10 s of vortex mixing each time, after which water was added. The volume fraction of particles in all these mixtures was between 1.17% and 1.29%, and the water/oil volume ratio was 39/61 or 40/60. All amounts were determined by weighing; volume fractions were calculated using the mass densities of PMMA (1.166 g mL^{-1}),[50] *n*-hexadecane (0.770 g mL^{-1}), and water (0.997 g mL^{-1}; density meter, Anton Paar, DMA 4500).

Sample mixtures were emulsified through 60 s of vortex mixing and stored at room temperature in a separate corner of a personal glass-door laboratory cabinet. Brightfield micrographs of the emulsions were recorded using Köhler illumination on an Olympus BX50 upright microscope, equipped with an Olympus 10×/0.20 NA objective and a QImaging QICam Fast 1394 camera (Qcapture Pro software set to 8-bit). Pixel size was calibrated using an 80 lines/mm grid, and droplets were sized using the "label and measure" feature of ImageJ. Emulsions were also characterized using digital photography using a FUJIFILM FinePix Z10fd and J210 camera (see the Supporting Information, SI).

For microscopy during bulk-emulsion rheology, to optimize image quality, index-matched PR emulsions were prepared using dried ASM408 (8 vol %).[5] The aqueous phase was a 60 wt % solution of sodium iodide in deionized water, the oil phase was a mixture of DC550 and CHB (DC550:CHB = 80.5:19.5 w/w), and the volume ratio aqueous/oil phase was 40/60; emulsification was achieved via vortex mixing. An appropriate amount of sample was then transferred onto the bottom plate of a rheometer, in this case a 50 mm diameter cover slide coated with PMMA particles and baked under vacuum at 120 °C (Gallenkamp Vacuum Oven); the cover slide was clamped onto a stage with a viewing hole. The rheometer used was a TA AR2000 and the top plate was a TA stainless steel 40 mm diameter plate (painted black to suppress reflections while imaging). To achieve single-particle resolution, we used a Nikon E Plan 100×/1.25 NA oil-immersion objective. The NBD in the PMMA particles was excited using a Cool LED pE system and videos were recorded using an Allied Manta camera (MG 033B ASG); emission filters were used as appropriate for NBD fluorescence.

RESULTS AND DISCUSSION

Interfacial Microscopy. As the particles have a radius $R \approx 0.5$ μm and are fluorescently labeled, we employ fluorescence microscopy to study the 2D structure and dynamics of the PMMA colloids at a flat water–oil interface. Figure 1a shows a micrograph of undried 0.455 μm radius PMMA colloids at a water–hexadecane interface. Many particles appear as singlets, though there are several interfacial aggregates as well. Particles were never detected in the water phase, but it was possible to observe nonsedimented particles in the oil phase whose motion was not restricted to the xy plane, i.e., parallel to the liquid interface; the region directly above the interface did, however, appear devoid of particles. To verify that the particles in Figure 1a are interfacial, the container was tapped and ethanol was added to the oil phase after the experiment, neither of which caused the particle layer to disappear (though we did observe transient in-plane motion and additional aggregates afterward). Interfacial aggregates are also observed if the particles are (i) dried after cleaning in hexane or (ii) left in hexane for ∼1 h or more before spreading. Furthermore, we have observed that the particles fully sediment in the spreading solvent hexane overnight, but appear stable in the oil phase hexadecane.

Intriguingly, the interfacial particles in Figure 1a are further apart than we had expected for maximum coverage, i.e., if all added particles would have attached to the liquid interface. This is confirmed by the radial distribution function $g(r)$ in Figure 1b, extracted from Figure 1a using image analysis, which shows an average interparticle spacing of ∼14R. Up to four maxima can be seen in this $g(r)$, suggesting some long-range order in the static structure of the interfacial particles. Combined with the particle-depleted zone just above the water–oil interface,

DOI: 10.1021/acs.langmuir.6b04365
Langmuir 2017, 33, 4107–4118

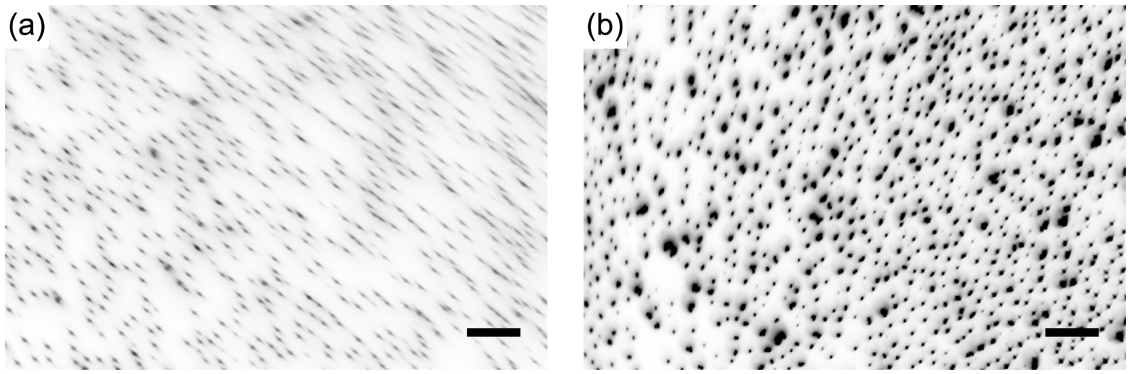

Figure 2. (a) Fluorescence micrograph of (a) undried and (b) dried 1.04 μm radius poly(methyl methacrylate) particles (dark) at a water−oil(dodecane) interface. Measured apparent surface coverage is (a) 0.09 and (b) 0.12; scale bar is 50 μm. The spherical particles seem elongated in (a) due to in-plane drift.

this implies a repulsive interaction between the interfacial particles beyond their steric repulsion (steric barrier ∼13 nm).[51] The interfacial particle dynamics corroborate the presence of a long-range interaction. From the mean squared displacement (Figure 1c), a particle diffusion coefficient of D = 0.10 $\mu m^2\ s^{-1}$ is calculated. This value is of the same order of magnitude as that observed for charge-stabilized microparticles at water−oil interfaces at similar surface coverage in the absence of salt;[52] any discrepancy can be explained by differences in oil viscosity and contact angle.[19,52]

These observations seem reminiscent of the long-range repulsion between interfacial particles observed by Aveyard et al.[37] and Masschaele et al.,[38] though both of these studies employed charge-stabilized rather than sterically stabilized particles. Aveyard et al. attribute this long-range repulsion to a small number of residual charges at the particle-oil interface,[37] whereas Masschaele et al. attribute it to the finite-size of the counterions and the resulting compact inner double layer.[38] Leunissen et al. observed long-range repulsion between PMMA−PHSA particles similar to the ones used here, but they employed apolar phases with relatively high dielectric constants that were prone to light-induced dissociation (CHB).[53] Admittedly, charge effects might play some role in our system, as the unreacted acid group at the end of the PHSA molecule could in principle dissociate. However, as far as we are aware, PMMA−PHSA particles are not stable in water, which seems to rule out extensive dissociation.

To show and quantify the effect of drying, we compare micrographs of undried (Figure 2a) and dried (Figure 2b) PMMA−PHSA particles at a water−oil interface. Despite the apparent elongation of spherical particles due to in-plane drift in Figure 2a, it is qualitatively clear that drying the particles results in interfacial layers with a greater degree of aggregation. To quantify this, we use image analysis to extract the apparent area of each interfacial entity (particle or aggregate) in Figure 2a,b. We then calculate the average $\langle A \rangle$ and corresponding polydispersity

$$\mathcal{D} = \frac{s}{\langle A \rangle} \cdot 100\% \tag{4}$$

where s is the standard deviation in A. The idea is that aggregates will lead to an increase in the number of larger-than-average entities, which leads to an increase in polydispersity. For the undried particles we find $\mathcal{D}_{\mathrm{undried}}$ = 69%, whereas for the dried particles we find $\mathcal{D}_{\mathrm{dried}}$ = 106%, which quantitatively confirms that drying the particles results in interfacial layers with a greater degree of aggregation. Note that these interfacial aggregates could be the result of particle aggregation at the interface, e.g., because the stabilizing PHSA layer has collapsed during drying and has not fully reflated yet, or it could be due to incomplete redispersion after drying.

Interfacial Compression−Expansion Experiments. A complementary method for probing the interactions between interfacial particles is by measuring surface pressure Π vs surface coverage Φ in a Langmuir trough. Figure 3a,b shows (Π, area) graphs for undried and dried PMMA−PHSA particles at a water−hexadecane interface. At large area, i.e., upon initial compression, the graphs are qualitatively similar (Figure 3b). Note, however, that we were not able to compress the water−oil interface laden with dried particles beyond buckling, i.e., that graph does not have an upper knee (Figure 3a).[31]

In order to quantitatively compare our data to existing literature, we convert our (Π, area) graphs to (Π, Φ) graphs. Based on verification of particle coverage determined by microscopy, we assume interfacially close-packed particles at an area fraction of Φ ≈ 0.86 at the lower bend,[54] i.e., the area at which the second derivative of the (Π, area) graph is maximum. The "undried" data is shown in Figure 3c as a (Π, Φ) graph, which compares favorably with measurements on undried PMMA−PHSA particles by Doroszkowski and Lambourn.[51]

Here, before close packing was reached, consistently higher surface pressures were recorded for compressed interfaces of dried vs undried particles, but the difference is relatively small (Figure 3a,b). This suggests that the (quasistatic) dilatational rheology of undried and dried PMMA−PHSA particles at water−hexadecane interfaces is similar. Moreover, Doroszkowski and Lambourn's data for PMMA particles with and without PHSA stabilizer are also similar approaching close-packing, reflecting an equivalent convergence of the dilatational rheology of stable and unstable particles. In the context of particle-stabilized emulsions formed through limited coalescence,[55] during which the particles at the droplet interface are only compressed once, one might therefore expect little difference between undried/stable and dried/unstable particles as long as interfacial shear rheology plays a minor role in this system.

As detailed in Figure 8 of the SI, distinct behavior of the different interfaces becomes much more clearly visible upon successive cycles of compression and expansion, wherein the higher state of aggregation of dried particles and thereby tendency to further associate means the interfaces of dried and redispersed particles show lower maximum attainable surface

DOI: 10.1021/acs.langmuir.6b04365
Langmuir 2017, 33, 4107−4118

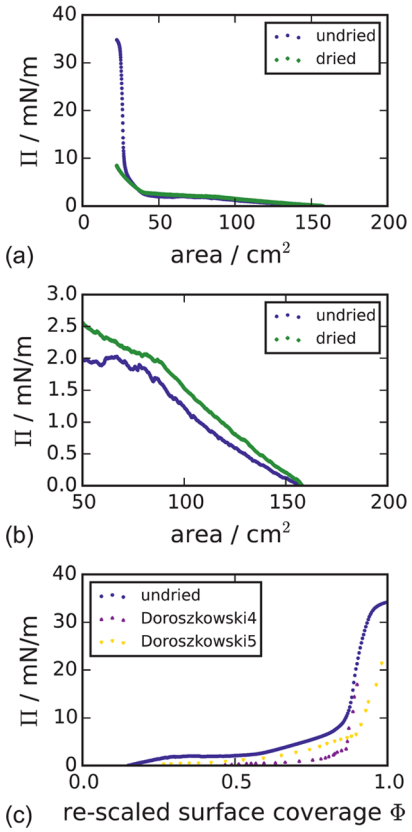

Figure 3. Compression measurements, performed in a Langmuir trough, of undried and dried 0.455 μm radius poly(methyl methacrylate) particles at a water−oil (hexadecane) interface: (a/b) surface pressure Π vs area available to interfacial particles; (b) is a zoom of (a). (c) Same "undried" data as in (a), but area has been converted to surface coverage (see text for details); our data is similar to "Doroszkowski4(5)", which is Langmuir-trough data on undried PMMA particles (5: without stabilizer) called "dispersion 4/5" in ref 51.

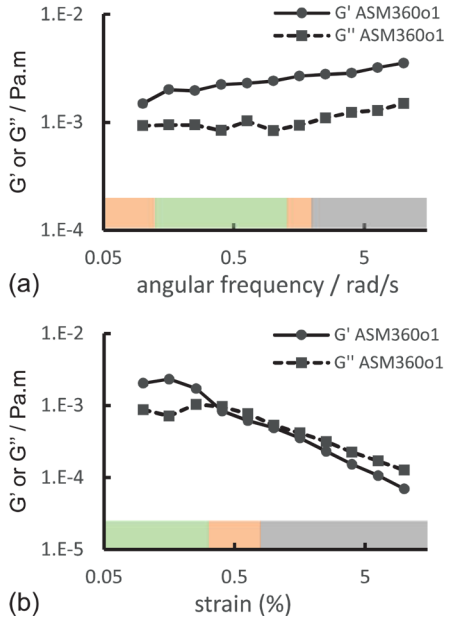

Figure 4. Oscillatory-shear rheology measurements of dried 0.575 μm radius poly(methyl methacrylate) particles at a water−oil (hexadecane) interface: (a) frequency sweep at a strain amplitude of 0.1% and (b) strain sweep at a frequency of 1 rad/s; maximum possible surface coverage is 0.88. Colored bars on horizontal axis, from left to right: measured stress/inertia stress is (green) > 10, (orange) > 5, and (gray) < 5 (see text for details).

pressures upon cycling and larger degrees of hysteresis than are observed from the more stable interfaces of undried particles.

Oscillatory-Shear Rheology. To probe the mechanical properties of the particle-laden water−oil interface under shear, we performed oscillatory-shear measurements using a double-wall ring setup. Figure 4a shows a frequency sweep at a strain amplitude of 0.1% for dried 0.575 μm radius PMMA−PHSA particles at a water−hexadecane interface. In the frequency range [0.1, 10] rad/s, $G' > G''$, suggesting that the interface is solid-like at this strain amplitude. The corresponding strain sweep at 1 rad/s in Figure 4b shows a transition to viscous behavior ($G'' > G'$) at strain amplitudes $\gamma > 0.5\%$. The corresponding shear yield stress $\sigma_y \sim 1 \times 10^{-3}$ Pa·m ·0.005 = 5 × 10^{-6} Pa·m.

It should be noted here that these oscillatory-shear measurements are challenging, because the moduli values are relatively low, for example 2 orders of magnitude lower than for monolayers of silica nanoparticles at water−air interfaces.[56] On the one hand, at low frequencies or strain amplitudes, the measured torque is close to the instrument resolution, so the signal-to-noise ratio is small. On the other hand, at large frequencies, the inertia of the geometry starts dominating the measured torque. Here, the solid-like behavior at low frequency/strain amplitude is in the "green" zone (Figure 4), but yielding and the viscous regime are in the "orange" and "gray" zones. This suggests that more sensitive measurements are required to back up these results and to measure the interfacial rheology of undried particles, which is why we turn to creep-recovery measurements below.

Creep-Recovery Rheology. *Creep-Recovery of Undried and Dried Particles.* To achieve higher sensitivity in the interfacial shear rheological measurements, we measured the creep-recovery response of undried and dried particles at a water−oil interface. The surface coverage of the interface is controlled by working at a fixed high-shear interfacial viscosity. The corresponding surface coverage can be estimated from a Krieger-Dougherty fit for the relative viscosity[28]

$$\eta_r = \left(1 - \frac{\phi_I}{\phi_{I,max}}\right)^{-[\eta]\phi_{I,max}} \quad (5)$$

The maximum packing in 2D, $\phi_{I,max}$, is taken as 0.86, as we did for the Langmuir-trough measurements, and the product of the intrinsic viscosity and maximum packing, $[\eta]\phi_{I,max}$, is taken as 1.9.[57] This gives a surface coverage of approximately 0.74 for our creep-recovery measurements.

Figure 5a shows the transient strain curves at different stresses for undried PMMA particles at a water−hexadecane interface at a surface coverage of 0.74. Qualitatively, all graphs look similar, showing an oscillatory strain response transforming into an elastic, solid-like response at long times. This elasticity is also seen in the recovery phase where a nearly complete recovery is observed, preceded by a transient oscillatory response. This oscillatory response is known as "creep ringing" and it occurs due to the coupling of the instrument's inertia with the sample elasticity under shear.[58] It was recently shown that it can also occur during interfacial rheological measurements and that the interfacial analogues of

DOI: 10.1021/acs.langmuir.6b04365
Langmuir 2017, 33, 4107−4118

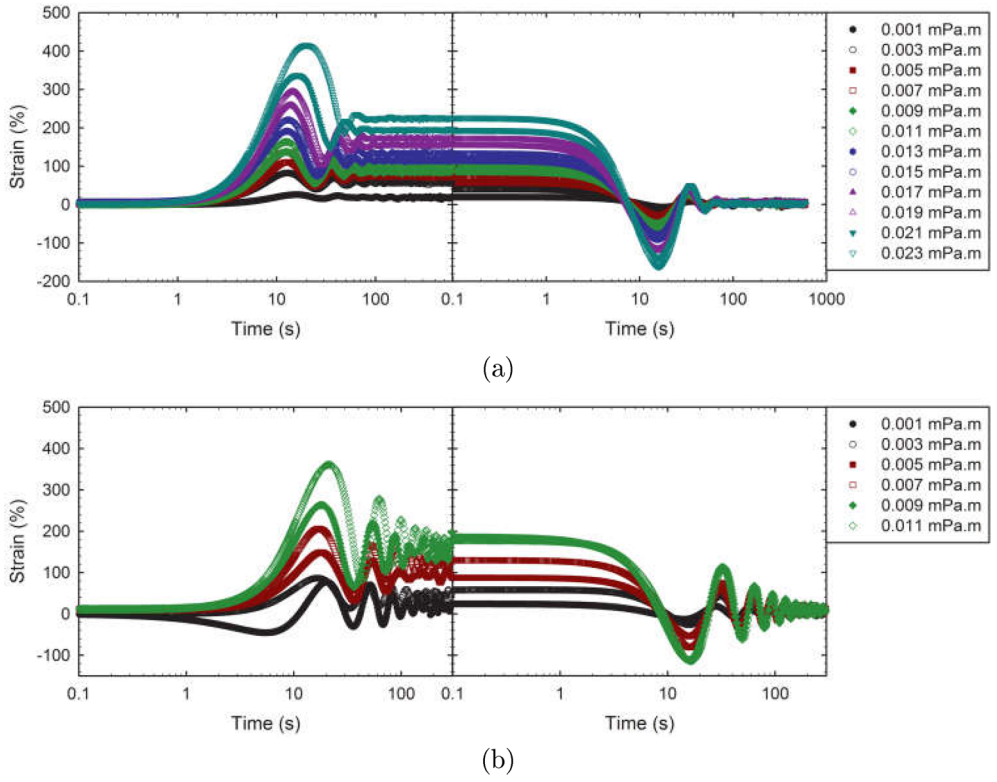

Figure 5. (a) Strain response during a creep-recovery experiment at a water-hexadecane interface, laden with undried 0.455 μm radius poly(methyl methacrylate) particles, using the normal double-wall ring; particle surface coverage $\phi \approx 0.74$. (b) Strain response during a creep-recovery experiment at a water−air interface, without particles, measured with the modified "thick" double-wall ring geometry.

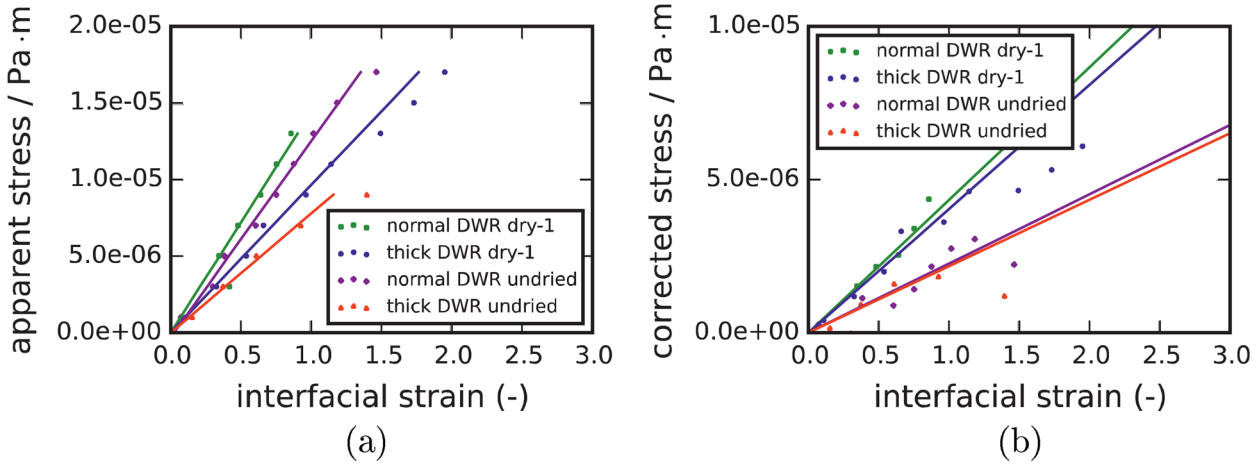

Figure 6. Steady-state stress−strain curves for 0.455 μm radius poly(methyl methacrylate) particles at a water−hexadecane interface, based on the data in Figure 5a and the SI: (a) apparent data and (b) corrected data.

the bulk rheological constitutive equations can be used to describe the behavior.[59] The transient strain curves for the dried particles and the thick ring can be found in the SI; the results are qualitatively similar but differ in the frequency of the ringing and the strain amplitude, which are both dependent on the viscoelastic properties of the sample and the measurement geometry.[58]

Following Jaishankar et al.,[59] the transient strain response can be described by

$$\epsilon(t) = \epsilon_f\left[1 - \exp(-\alpha t)\left(\cos(\omega t) + \frac{\alpha}{\omega}\sin(\omega t)\right)\right] \quad (6)$$

where α, ω, and ϵ_f are given by

$$\alpha = \frac{b\eta}{2I}$$

$$\omega = \sqrt{\frac{G}{I/b} - \left(\frac{b\eta}{2I}\right)^2}$$

$$\epsilon_f = \frac{\sigma_0}{G}$$

This response is derived by considering a Kelvin−Voigt model (for the sample) in series with the inertia of the measurement system. In these equations, ϵ is the strain, G and η are the

DOI: 10.1021/acs.langmuir.6b04365
Langmuir 2017, 33, 4107−4118

elastic and viscous constant in the Kelvin−Voigt model, I is the inertia of the measurement system, σ_0 the applied stress, and b is a geometrical constant defined as the ratio of the strain and stress constant of the measurement geometry. Note that oscillations during a creep experiment can only occur when the elasticity of the system is sufficiently high:[58]

$$G > \frac{b\eta^2}{4I} \tag{7}$$

Equation 6 has been used to fit each strain-time curve in Figure 5a (not shown here). Similar to Jaishankar et al.,[59] we notice that the model is able to quantitatively replicate either the short-term behavior or the long-term behavior correctly, but not both at the same time. This suggests that the Kelvin−Voigt model, with only one characteristic material time scale, is probably too simplistic in describing the full dynamic behavior of the particle-laden interface. The data can then be summarized by plotting the applied stress versus the steady-state strain as shown in Figure 6a; it also shows the results for the dried particles and the thick DWR ring. A linear relation is found between stress and strain confirming again the solid-like behavior of the system with a constant modulus at low stresses shown as the lines in Figure 6a. These curves, however, can only be used to derive the apparent interfacial modulus, as they are clearly affected by the geometry compliance. Indeed, the response of PMMA interfacial layers, both undried and dried PMMA particles, depends on the ring used.

We propose a basic correction for the observed geometry dependence of the interfacial moduli (see below for details). The combined effect of subphase and geometry compliance at low *Bo* can be corrected for by subtracting the measured modulus of the bare interfaces from the apparent data for the particle-laden ones. This is shown in Figure 6b, where again the lines are a linear fit to the data, from which the actual modulus of the interfacial layers can be derived (see Table 1).

Table 1. Apparent and Corrected Interfacial Moduli for Dried and Undried 0.455 μm Radius Poly(methyl methacrylate) Particles at a Water−Hexadecane Interface[a]

	apparent G_s/ 10^{-6} Pa m	corrected G_s/ 10^{-6} Pa m
ring 1 PMMA undried	12.8	2.3
ring 2 PMMA undried	7.8	2.2
ring 1 PMMA dry-1	14.4	4.33
ring 2 PMMA dry-1	9.6	4.1
ring 1 PMMA dry-2	58.7	48.6
ring 1 PMMA dry-1 ($\phi \approx \phi_{max}$)	620	610

[a]Surface coverage is 0.74 unless stated otherwise; ring 1 is the normal ring, ring 2 is the thick ring (see text for details).

Importantly, the response of the interfacial layers is now independent of the geometry used, which provides validation for our empirical correction. A higher modulus is observed for the dried PMMA interfacial layers, though the difference between dried and undried particles is limited. Moreover, these moduli are low compared to other particle-laden systems;[34,56,60] that is, these PMMA layers show a weak elastic response under shear.

Correction for Geometry Dependence. Before presenting the effects of particle drying and concentration, we present here further details on the correction for the observed geometry dependence for the benefit of the initiated reader. The observation that the interfacial modulus is only an apparent one and that it depends on the measurement geometry used led us to measure the creep-recovery response of bare water−air and water−oil interfaces. The creep-recovery response of a bare water−air interface, measured with the thick geometry is shown in Figure 5b. Clearly, this bare interface shows an unexpected elastic response, e.g., highlighted by the creep ringing; only at the highest stresses measured, a viscous response was recovered. Since a water−air interface itself cannot show any elasticity, the source of the observed elasticity is not evident. Vandebril et al.[28] have shown that, in the limit of low *Bo* numbers (as is the case here), the interfacial deformation profile can significantly deviate from the expected linear one. In the case of oscillatory experiments for a viscous interface at low *Bo*, they showed that the resulting deformation profile has both in-phase and out-of-phase contributions. In other words, the presence of the subphase can cause an apparent elastic response at low *Bo* for viscous interfaces.

Qualitatively similar results were found for the standard DWR at water−air interfaces without particles, i.e., also showing creep ringing. The apparent elastic modulus of the bare interfaces can be calculated by taking the derivative of the stress with the steady state strain. The value of the apparent elastic moduli differ, however, for the standard and the thick DWR ring, indicating that the deformation profile at the interface depends on the stiffness of the geometry, at least at low *Bo*. The apparent elastic modulus measured with the standard geometry has a value of $(10.1 \pm 1.5) \times 10^{-6}$ Pa m, whereas for the thick ring a modulus of $(5.6 \pm 0.9) \times 10^{-6}$ Pa m was found. The overall higher apparent compliance of the thick ring is a consequence of the combined effects of the true intrinsic compliance of the ring and the occurrence of an out-of-phase component in the velocity field at the interface, due to the coupling of the interfacial deformation with the subphase. Due to the inherent nonlinear nature of the latter problem,[61] at equal stress amplitude a stiffer ring leads to a more nonlinear profile (a lower *Bo* number), and counterintuitively, a larger apparent compliance can then be observed experimentally. Quantitative agreement for the apparent elastic modulus was found when repeating the experiments at the water−hexadecane interface, confirming that the observed elasticity is indeed due to a complex interplay between the geometry stiffness and the subphase drag, i.e., not related to the interfacial tension. It should be noted that these measurements are extremely sensitive and not all measurements show ringing as pronounced as in Figure 5b. Given the sensitivity to the details of the geometry, the reported values of the apparent modulus should be handled with care for other DWRs and set-ups.

Effect of Particle Drying and Concentration. We also present the results of creep-recovery experiments on the effect of the drying protocol and particle concentration as obtained with ring 1 (normal DWR), since it has the lowest inertia and lowest apparent compliance. Figure 7 shows the steady-state stress−strain curves for a water−hexadecane interface laden with PMMA particles that have been dried normally and more severely. It is apparent that drying more severely leads to a stiffer interface compared to the undried particles and the less dried particles, i.e., the steady-state strains attained are significantly lower. Furthermore, the ringing shows a higher frequency and appears to be more regular (SI). Similarly, increasing the particle concentration leads to a more rigid interfacial layer. Remarkably, at this highest particle concentration, the strain is not completely recovered (SI). Note that,

DOI: 10.1021/acs.langmuir.6b04365
Langmuir 2017, 33, 4107−4118

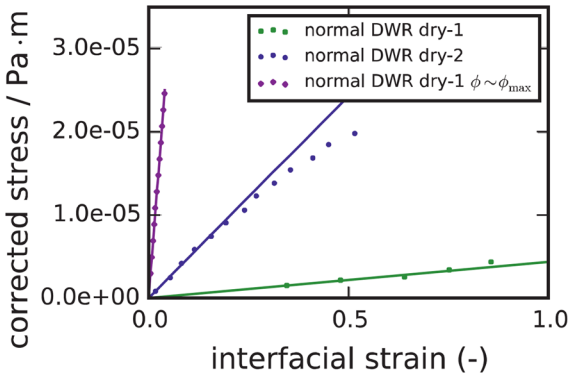

Figure 7. Corrected steady-state stress−strain curves of water−hexadecane interfaces laden with dried 0.455 μm radius poly(methyl methacrylate) particles, measured using the normal double-wall ring: effect of the extent of drying and particle concentration.

for these stiffer interfaces, the correction for the combined effect of subphase and geometry compliance is only a minor one.

Our creep-recovery results indicate that the history of the PMMA particles affects the corresponding interfacial rheology. Interfacial layers prepared with undried particles show a weak solid-like response, hardly above the geometry compliance at a surface coverage of approximately 0.74. Drying of the particles, and the extent of drying, have a strong effect on the interfacial layers, rigidifying them significantly. Microscopy observations show a larger degree of interfacial aggregation when using dried particles (Figure 2), which could be due to incomplete redispersion i.e. irreversible aggregation due to van der Waals forces. However, to the best of our knowledge, the effects of drying on the PHSA layer have not been reported previously. It is usually assumed that the PHSA layer collapses upon drying to form a layer about 6 to 7 nm thick, which is deemed too thin for effective stabilization. As PMMA−PHSA particles can be (at least to some degree) resuspended, it is generally assumed that the PHSA layer partly reflates when the particles are put back in a good solvent (e.g., *n*-hexadecane), but the required time-scale and whether it also happens at the aqueous side of the interface is unclear. In any case, the contact line around an interfacial aggregate is likely to be undulated, which may cause long-range capillary attractions. The long-range nature of these attractions might also explain the observed high recoverable elastic strain (up to ~200%).

Pickering-Emulsion Stability. To check whether the difference in interfacial shear rheology between undried and dried particles translates into a difference in shelf life between the corresponding particle-stabilized emulsions, we prepared water-in-hexadecane emulsions stabilized by undried particles (samples "w1" and "w2") or dried particles (samples "d1" and "d2") and monitored them over time. Figure 8 shows optical micrographs of these emulsions over a time period of 334 days (see SI for corresponding photographs). From such micrographs, emulsion stability can be monitored via droplet size; that is, an increase in the average droplet size suggests coalescence. We do not discern any qualitative difference in average droplet size between emulsions stabilized by undried or dried particles; this corroborates our observations based on macroscopic photographs (see SI). Thus, for water-in-hexadecane emulsions stabilized by PMMA−PHSA colloids, the difference in interfacial shear rheology between undried and dried particles does not seem to translate into a difference in

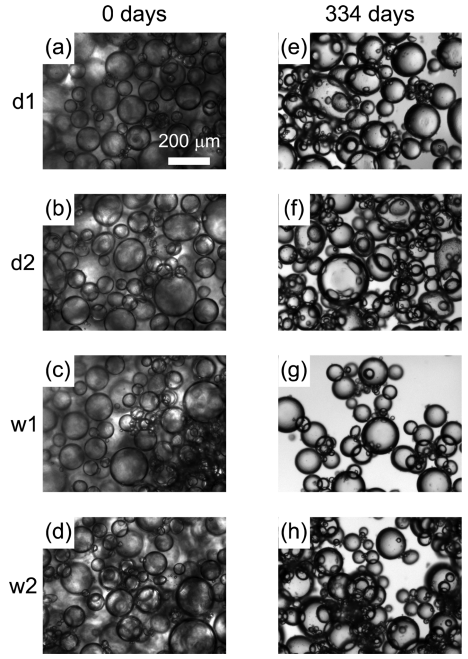

Figure 8. Optical micrographs of water-in-oil (hexadecane) emulsions, stabilized by "d" dried or "w" undried poly(methyl methacrylate) particles of radius 0.455 μm, at an age of (a−d) 0 days and (e−h) 334 days. From these micrographs, average droplet diameter is (a) 63 μm, (e) 62 μm, (d) 65 μm, and (h) 52 μm.

stability in the corresponding (quiescent) emulsions, at least not for the first 334 days.

Interestingly, our results may explain some paradoxical results in the literature. Working mainly with (charge-stabilized) silica nanoparticles Binks et al. have claimed that particles that flocculate in the continuous phase make for more stable PR emulsions,[10,11,62] possibly because the degree of flocculation affects wettability.[63,64] However, French has claimed that this is not necessarily true.[13] In a recent paper, Ridel and co-workers also reported that they have stabilized emulsions using charge-stabilized silica particles that do not aggregate in the bulk.[65] Bearing in mind that we use sterically stabilized rather than charge-stabilized particles, our results confirm that stable PR emulsions do not necessarily require particles that tend to aggregate in the continuous phase (Figure 8). However, they also suggest that only a few interfacial aggregates can already make the interface much stronger (Table 1); that is, aggregates would not be required for stable emulsions, but they can increase the stiffness of the interface, thereby promoting emulsion stability (even if the particles do not aggregate in bulk).

To check whether our PMMA particles aggregate once at the liquid−liquid interface of a droplet, we inspect microscopy videos recorded during (bulk) oscillatory shear on similar but transparent PR emulsions. Figure 9 shows snapshots from such a video of an emulsion consisting of water droplets (65 wt % NaI) in mainly silicone oil (DC550/CHB = 83/17 w/w), stabilized by fluorescent PMMA particles. We employ these transparent PR emulsions to facilitate fluorescence microscopy and, as far as we are aware, they behave similarly to water-dodecane/PMMA emulsions.[5] In particular, the presence of salt does not seem to lead to aggregation at the interface in this system, as demonstrated by the registering of red and green particles in Figure 7b of Maurice et al.[5] Notably, the

DOI: 10.1021/acs.langmuir.6b04365
Langmuir 2017, 33, 4107−4118

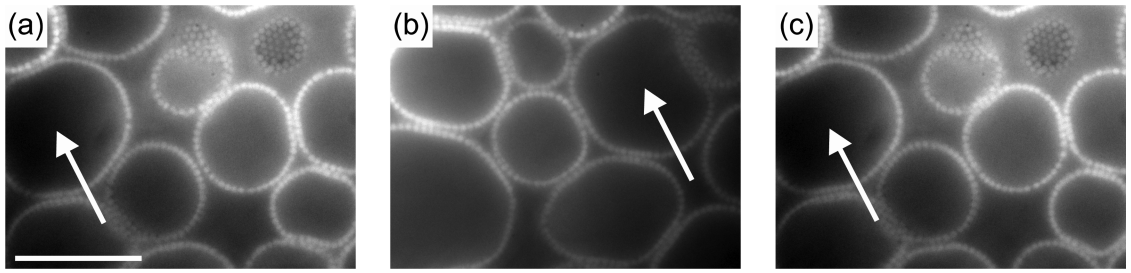

Figure 9. Micrographs of a water-in-oil(see text for details) emulsion stabilized by fluorescent poly(methyl methacrylate) particles (white) during oscillatory shear: (a) time $t = T$, (b) $t = (1 + 0.48)\ T$, and (c) $t = (1 + 0.99)\ T$, with T the period of oscillation. The white arrow points to the same droplet in each panel. Note the monolayer of PMMA particles at the droplet surface, which bends inward when pushed by a neighboring droplet, but also recovers afterward. Scale bar is 50 μm.

observation of registering of particles on touching droplets also implies that the particles have not aggregated in the form of fractals.

In Figure 9, note that the droplets are covered in a monolayer of PMMA particles; we have previously shown that these are close-packed in this and similar system(s).[5,17] This monolayer provides a mechanical barrier vs coalescence; that is, the aqueous phases of the droplets cannot merge because the particles keep them apart (see arrow in Figure 9b). Second, focusing on a single droplet (see arrow), the particle-coated droplet surface can bend inward when pushed by a neighboring droplet and it can recover afterward. Both these observations suggest that the PMMA particles at the droplet surface are not aggregated, corroborating our previous statement that, at least for our PR emulsions, the particles do not need to aggregate to form stable emulsions. This is not to say, of course, that interfacial rheology does not play any role in PR stability, especially when considering nonquiescent conditions.

Note that interfacial-shear rheology measurements probe only the extra stress due to the presence of the particulate layer. They are only a predictor of the stability of PR emulsions if that stability is dominated by the extra stress. For example, claims by Binks et al. that charge-stabilized nanoparticles that flocculate in the continuous phase make for more stable PR emulsions[10,11,62−64] align with relatively high interfacial-shear moduli measured for these particles at water−air interfaces by Zang et al.,[56] who also reported Brewster-angle micrographs of fracture of these monolayers upon compression. Indeed, Reynaert et al. showed that networks of aggregated particles at water−oil interfaces have solid-like rheological properties at relatively low surface coverage, but they are brittle monolayers; that is, they have a relatively small yield strain meaning that they break or shatter at relatively low strain.[34] In contrast, we have shown that our sterically stabilized PMMA−PHSA particles at water−oil interfaces form monolayers that (i) have relatively low interfacial-shear moduli (Table 1), (ii) are not brittle (Figure 9), and (iii) generate large surface pressures upon compression to close packing even for nonaggregating, undried particles (Figure 3). Hence, we suggest here that the stability of our sterically stabilized PR emulsions is dominated by dilatational rheology and, as such, (i) aggregation of particles does not significantly enhance PR emulsion stability and (ii) interfacial shear rheology is not a predictor for it.

SUMMARY AND CONCLUSIONS

We have presented a comprehensive set of interfacial-microscopy and interfacial-rheology measurements of micron-sized, sterically stabilized (PMMA−PHSA) particles at a water−oil interface. Interfacial microscopy of undried particles shows unexpectedly low surface coverage and Brownian-like motion, suggesting that the interparticle potential has a (long-range) repulsive component; interfacial microscopy of dried particles shows a larger degree of aggregation. Surface pressure−area measurements show that these monolayers generate large surface pressures upon compression to close packing, even for nonaggregating, i.e., undried particles, and microscopy videos of water-in-oil emulsions stabilized by similar particles under oscillatory shear show that they are not brittle. Interfacial oscillatory-shear measurements on dried particles reveal a weak 2D solid, though these measurements are challenging due to the relatively high geometry inertia. For creep-recovery measurements, we present an empirical method to correct for the combined effect of the subphase drag and the compliance of the double-wall ring geometry, which makes a significant contribution to the apparent elasticity of weak interfaces; we demonstrate that it can indeed explain differences in creep-recovery experiments with different rings. These measurements also show that drying the particles prior to spreading at the interface, and (especially) increasing the concentration of interfacial particles, makes for stiffer particle-laden interfaces; we attribute the former to capillary interactions induced by interfacial aggregates that are a result of incomplete redispersion of dried particles and/or transient collapse of the stabilizing layer at the particle's surface.

However, we have not observed a difference in quiescent stability of water-in-oil emulsions stabilized by undried or dried particles for over 11 months. Our results suggest that the stability of our Pickering emulsions is dominated by other factors, such as aspects of the dilatational interfacial rheology. In short, particles do not necessarily need to aggregate in bulk in order to form stable Pickering emulsions, but interfacial aggregates do make for stiffer interfaces; this may indeed be pivotal in systems where the stability of Pickering emulsions relies on shear interfacial rheology.

ASSOCIATED CONTENT

Supporting Information

The Supporting Information is available free of charge on the ACS Publications website at DOI: 10.1021/acs.langmuir.6b04365.

(1) Microscopy video of interfacial particles, (2) strain response for various interfaces during creep-recovery, (3) digital photographs of Pickering emulsions after 5, 41, and 334 days, and (4) Langmuir-trough data for three subsequent cycles. (ZIP)

DOI: 10.1021/acs.langmuir.6b04365
Langmuir 2017, 33, 4107−4118

AUTHOR INFORMATION

Corresponding Author

*E-mail: j.h.j.thijssen@ed.ac.uk. Phone: +44 (0)131 6505274.

ORCID

Jan Vermant: 0000-0002-0352-0656

Present Address

[‖]Emulco, Henri Farmanstraat 25, Ghent, B-9000, Belgium.

Notes

The data corresponding to this paper will be made available at http://dx.doi.org/10.7488/ds/1997.

The authors declare no competing financial interest.

ACKNOWLEDGMENTS

The authors thank Ali Mohraz for help with the bulk rheo-imaging experiments and Iain Muntz for recording the micrographs in Figure 2. We also thank Jan Mewis, Michiel Hermes, and TA Instruments for useful discussions. V.B. acknowledges financial support from the European Seventh Framework Project 2012-316866 "Soft Matter At Aqueous Interfaces" (SOMATAI). A.B.S. acknowledges financial support by EPSRC Grant No. EP/J007404. J.H.J.T. acknowledges the European Soft Matter Infrastructure (ESMI) for a travel grant, the Royal Society of Edinburgh/BP Trust Personal Research Fellowship for funding, and The University of Edinburgh for a Chancellor's Fellowship.

REFERENCES

(1) Madivala, B.; Vandebril, S.; Fransaer, J.; Vermant, J. Exploiting particle shape in solid stabilized emulsions. *Soft Matter* **2009**, *5*, 1717−1727.

(2) Hermes, M.; Clegg, P. S. Yielding and flow of concentrated Pickering emulsions. *Soft Matter* **2013**, *9*, 7568−7575.

(3) Fuller, G. G.; Vermant, J. Complex Fluid-Fluid Interfaces: Rheology and Structure. *Annu. Rev. Chem. Biomol. Eng.* **2012**, *3*, 519−543.

(4) Binks, B. P., Horozov, T. S., Eds.; *Colloidal Particles at Liquid Interfaces*; Cambridge University Press: Cambridge, U.K., 2006.

(5) Maurice, L.; Maguire, R. A.; Schofield, A. B.; Cates, M. E.; Clegg, P. S.; Thijssen, J. H. J. Squeezing particle-stabilized emulsions into biliquid foams - equation of state. *Soft Matter* **2013**, *9*, 7757−7765.

(6) Cates, M. E.; Clegg, P. S. Bijels: a new class of soft materials. *Soft Matter* **2008**, *4*, 2132−2138.

(7) Hunter, T. N.; Pugh, R. J.; Franks, G. V.; Jameson, G. J. The role of particles in stabilising foams and emulsions. *Adv. Colloid Interface Sci.* **2008**, *137*, 57−81.

(8) Leal-Calderon, F.; Schmitt, V. Solid-stabilized emulsions. *Curr. Opin. Colloid Interface Sci.* **2008**, *13*, 217−227.

(9) Cai, D.; Thijssen, J. H. J.; Clegg, P. S. Making Non-aqueous High Internal Phase Pickering Emulsions: Influence of Added Polymer and Selective Drying. *ACS Appl. Mater. Interfaces* **2014**, *6*, 9214−9219.

(10) Binks, B. P.; Lumsdon, S. O. Catastrophic phase inversion of water-in-oil emulsions stabilized by hydrophobic silica. *Langmuir* **2000**, *16*, 2539−2547.

(11) Binks, B. P.; Whitby, C. P. Nanoparticle silica-stabilised oil-in-water emulsions: improving emulsion stability. *Colloids Surf., A* **2005**, *253*, 105−115.

(12) Bizmark, N.; Ioannidis, M. A. Effects of Ionic Strength on the Colloidal Stability and Interfacial Assembly of Hydrophobic Ethyl Cellulose Nanoparticles. *Langmuir* **2015**, *31*, 9282−9289.

(13) French, D. J. *Fundamental Aspects of Pickering Emulsion Stabilization*. Ph.D. thesis, The University of Edinburgh, 2015.

(14) Ho, K. W.; Ooi, C. W.; Mwangi, W. W.; Leong, W. F.; Tey, B. T.; Chan, E. S. Comparison of self-aggregated chitosan particles prepared with and without ultrasonication pretreatment as Pickering emulsifier. *Food Hydrocolloids* **2016**, *52*, 827−837.

(15) Aveyard, R.; Binks, B. P.; Clint, J. H. Emulsions stabilised solely by colloidal particles. *Adv. Colloid Interface Sci.* **2003**, *100*, 503−546.

(16) Goebel, A.; Lunkenheimer, K. Interfacial tension of the water/n-alkane interface. *Langmuir* **1997**, *13*, 369−372.

(17) Thijssen, J. H. J.; Schofield, A. B.; Clegg, P. S. How do (fluorescent) surfactants affect particle-stabilized emulsions? *Soft Matter* **2011**, *7*, 7965−7968.

(18) Isa, L.; Lucas, F.; Wepf, R.; Reimhult, E. Measuring single-nanoparticle wetting properties by freeze-fracture shadow-casting cryo-scanning electron microscopy. *Nat. Commun.* **2011**, *2*, 438.

(19) Lide, D. R., Ed.; *CRC Handbook of Chemistry and Physics*; CRC Press: Boca Raton, FL, 2001−2002.

(20) Clegg, P. S.; Herzig, E. M.; Schofield, A. B.; Egelhaaf, S. U.; Horozov, T. S.; Binks, B. P.; Cates, M. E.; Poon, W. C. K. Emulsification of partially miscible liquids using colloidal particles: Nonspherical and extended domain structures. *Langmuir* **2007**, *23*, 5984−5994.

(21) Zang, D. Y.; Rio, E.; Delon, G.; Langevin, D.; Wei, B.; Binks, B. P. Influence of the contact angle of silica nanoparticles at the air-water interface on the mechanical properties of the layers composed of these particles. *Mol. Phys.* **2011**, *109*, 1057−1066.

(22) Imperiali, L.; Liao, K. H.; Clasen, C.; Fransaer, J.; Macosko, C. W.; Vermant, J. Interfacial Rheology and Structure of Tiled Graphene Oxide Sheets. *Langmuir* **2012**, *28*, 7990−8000.

(23) Miller, R.; Wustneck, R.; Kragel, J.; Kretzschmar, G. Dilational and shear rheology of adsorption layers at liquid interfaces. *Colloids Surf., A* **1996**, *111*, 75−118.

(24) Derkach, S. R.; Kragel, J.; Miller, R. Methods of Measuring Rheological Properties of Interfacial Layers (Experimental Methods of 2D Rheology). *Colloid J.* **2009**, *71*, 1−17.

(25) Kragel, J.; Derkatch, S. R. Interfacial shear rheology. *Curr. Opin. Colloid Interface Sci.* **2010**, *15*, 246−255.

(26) Brooks, J. H.; Pethica, B. A. Properties of Ionized Monolayers 0.6. Film Pressures of Ionized Spread Monalayers at Heptane/Water Interface. *Trans. Faraday Soc.* **1964**, *60*, 208.

(27) Murray, B. S.; Nelson, P. V. A novel Langmuir trough for equilibrium and dynamic measurements on air-water and oil-water monolayers. *Langmuir* **1996**, *12*, 5973−5976.

(28) Vandebril, S.; Franck, A.; Fuller, G. G.; Moldenaers, P.; Vermant, J. A double wall-ring geometry for interfacial shear rheometry. *Rheol. Acta* **2010**, *49*, 131−144.

(29) Zang, D. Y.; Rio, E.; Langevin, D.; Wei, B.; Binks, B. P. Viscoelastic properties of silica nanoparticle monolayers at the air-water interface. *Eur. Phys. J. E: Soft Matter Biol. Phys.* **2010**, *31*, 125−134.

(30) Petkov, J. T.; Gurkov, T. D.; Campbell, B. E.; Borwankar, R. P. Dilatational and shear elasticity of gel-like protein layers on air/water interface. *Langmuir* **2000**, *16*, 3703−3711.

(31) Aveyard, R.; Clint, J. H.; Nees, D.; Quirke, N. Structure and collapse of particle monolayers under lateral pressure at the octane/aqueous surfactant solution interface. *Langmuir* **2000**, *16*, 8820−8828.

(32) Samaniuk, J. R.; Vermant, J. Micro and macrorheology at fluid-fluid interfaces. *Soft Matter* **2014**, *10*, 7023−7033.

(33) Edwards, D. A.; Brenner, H.; Wasan, D. T. *Interfacial Transport Processes and Rheology*; Butterworth-Heinemann: Boston, 1991.

(34) Reynaert, S.; Moldenaers, P.; Vermant, J. Interfacial rheology of stable and weakly aggregated two-dimensional suspensions. *Phys. Chem. Chem. Phys.* **2007**, *9*, 6463−6475.

(35) Barman, S.; Christopher, G. F. Simultaneous Interfacial Rheology and Microstructure Measurement of Densely Aggregated Particle Laden Interfaces Using a Modified Double Wall Ring Interfacial Rheometer. *Langmuir* **2014**, *30*, 9752−9760.

(36) Barman, S.; Christopher, G. F. Role of capillarity and microstructure on interfacial viscoelasticity of particle laden interfaces. *J. Rheol.* **2016**, *60*, 35−45.

(37) Aveyard, R.; Binks, B. P.; Clint, J. H.; Fletcher, P. D. I.; Horozov, T. S.; Neumann, B.; Paunov, V. N.; Annesley, J.; Botchway, S. W.; Nees, D.; Parker, A. W.; Ward, A. D.; Burgess, A. N. Measurement of

DOI: 10.1021/acs.langmuir.6b04365
Langmuir 2017, 33, 4107−4118

long-range repulsive forces between charged particles at an oil-water interface. *Phys. Rev. Lett.* **2002**, *88*, 246102.
(38) Masschaele, K.; Park, B. J.; Furst, E. M.; Fransaer, J.; Vermant, J. Finite Ion-Size Effects Dominate the Interaction between Charged Colloidal Particles at an Oil-Water Interface. *Phys. Rev. Lett.* **2010**, *105*, 048303.
(39) Bosma, G.; Pathmamanoharan, C.; de Hoog, E. H. A.; Kegel, W. K.; van Blaaderen, A.; Lekkerkerker, H. N. W. Preparation of monodisperse, fluorescent PMMA-latex colloids by dispersion polymerization. *J. Colloid Interface Sci.* **2002**, *245*, 292−300.
(40) Bryant, G.; Williams, S. R.; Qian, L.; Snook, I. K.; Perez, E.; Pincet, F. How hard is a colloidal "hard-sphere" interaction? *Phys. Rev. E: Stat. Phys., Plasmas, Fluids, Relat. Interdiscip. Top.* **2002**, *66*, 060501.
(41) Note that the terms "aggregation", "flocculation", and "agglomeration" appear to be used interchangeably in the literature.[66,67] In analogy with literature on fumed silica, we use "agglomeration" for particle assemblies that can be broken up into its smaller subunits by ultrasonication and "aggregation" for those that cannot.
(42) Dickinson, E.; Ettelaie, R.; Kostakis, T.; Murray, B. S. Factors controlling the formation and stability of air bubbles stabilized by partially hydrophobic silica nanoparticles. *Langmuir* **2004**, *20*, 8517−8525.
(43) Whitby, C. P.; Krebsz, M. Coalescence in concentrated Pickering emulsions under shear. *Soft Matter* **2014**, *10*, 4848−4854.
(44) Murray, B. S.; Phisarnchananan, N. The effect of nanoparticles on the phase separation of waxy corn starch plus locust bean gum or guar gum. *Food Hydrocolloids* **2014**, *42*, 92−99.
(45) Vargaftik, N. B.; Volkov, B. N.; Voljak, L. D. International Tables of the Surface-Tension of Water. *J. Phys. Chem. Ref. Data* **1983**, *12*, 817−820.
(46) Rolo, L. I.; Caco, A. I.; Queimada, A. J.; Marrucho, I. M.; Coutinho, J. A. P. Surface tension of heptane, decane, hexadecane, eicosane, and some of their binary mixtures. *J. Chem. Eng. Data* **2002**, *47*, 1442−1445.
(47) Isa, L. private communication, 2017.
(48) Paunov, V. N. Novel method for determining the three-phase contact angle of colloid particles adsorbed at air-water and oil-water interfaces. *Langmuir* **2003**, *19*, 7970−7976.
(49) Rasband, W. accessed 2015; http://fiji.sc/Fiji.
(50) Campbell, A. I.; Bartlett, P. Fluorescent hard-sphere polymer colloids for confocal microscopy. *J. Colloid Interface Sci.* **2002**, *256*, 325−330.
(51) Doroszkowski, A.; Lambourn, R. Measurement of Strength of Steric Barriers in Non-Aqueous Polymer Dispersions. *J. Polym. Sci., Part C: Polym. Symp.* **1971**, *34*, 253−264.
(52) Ortega, F.; Ritacco, H.; Rubio, R. G. Interfacial microrheology: Particle tracking and related techniques. *Curr. Opin. Colloid Interface Sci.* **2010**, *15*, 237−245.
(53) Leunissen, M. E.; van Blaaderen, A.; Hollingsworth, A. D.; Sullivan, M. T.; Chaikin, P. M. Electrostatics at the oil-water interface, stability, and order in emulsions and colloids. *Proc. Natl. Acad. Sci. U. S. A.* **2007**, *104*, 2585−2590.
(54) Maestro, A.; Deshmukh, O. S.; Mugele, F.; Langevin, D. Interfacial Assembly of Surfactant-Decorated Nanoparticles: On the Rheological Description of a Colloidal 2D Glass. *Langmuir* **2015**, *31*, 6289−6297.
(55) Arditty, S.; Schmitt, V.; Lequeux, F.; Leal-Calderon, F. Interfacial properties in solid-stabilized emulsions. *Eur. Phys. J. B* **2005**, *44*, 381−393.
(56) Zang, D. Y.; Langevin, D.; Binks, B. P.; Wei, B. B. Shearing particle monolayers: Strain-rate frequency superposition. *Phys. Rev. E* **2010**, *81*, 011604.
(57) Tao, R.; Xu, X. Reducing the viscosity of crude oil by pulsed electric or magnetic field. *Energy Fuels* **2006**, *20*, 2046−2051.
(58) Ewoldt, R. H.; McKinley, G. H. Creep Ringing in Rheometry or How to Deal with Oft-discarded Data in Step Stress Tests! *Rheol. Bull.* **2007**, *76*, 4−6.
(59) Jaishankar, A.; Sharma, V.; McKinley, G. H. Interfacial viscoelasticity, yielding and creep ringing of globular protein-surfactant mixtures. *Soft Matter* **2011**, *7*, 7623−7634.
(60) Van Hooghten, R.; Imperiali, L.; Boeckx, V.; Sharma, R.; Vermant, J. Rough nanoparticles at the oil-water interfaces: their structure, rheology and applications. *Soft Matter* **2013**, *9*, 10791−10798.
(61) Reynaert, S.; Brooks, C. F.; Moldenaers, P.; Vermant, J.; Fuller, G. G. Analysis of the magnetic rod interfacial stress rheometer. *J. Rheol.* **2008**, *52*, 261−285.
(62) Binks, B. P. Particles as surfactants - similarities and differences. *Curr. Opin. Colloid Interface Sci.* **2002**, *7*, 21−41.
(63) Binks, B. P.; Philip, J.; Rodrigues, J. A. Inversion of silica-stabilized emulsions induced by particle concentration. *Langmuir* **2005**, *21*, 3296−3302.
(64) Binks, B. P.; Fletcher, P. D. I.; Holt, B. L.; Beaussoubre, P.; Wong, K. Phase inversion of particle-stabilised perfume oil-water emulsions: experiment and theory. *Phys. Chem. Chem. Phys.* **2010**, *12*, 11954−11966.
(65) Ridel, L.; Bolzinger, M. A.; Gilon-Delepine, N.; Dugas, P. Y.; Chevalier, Y. Pickering emulsions stabilized by charged nanoparticles. *Soft Matter* **2016**, *12*, 7564−7576.
(66) Verwey, E. J. W.; Overbeek, J. T. G. *Theory of the Stability of Lyophobic Colloids*; Dover Publications, Inc.: Mineola, NY, 1999.
(67) Jones, R. A. L. *Soft Condensed Matter*; Oxford University Press: Oxford (UK), 2007.

DOI: 10.1021/acs.langmuir.6b04365
Langmuir 2017, 33, 4107−4118